JOURNAL OF Materials CHEMISTRY

Effect of colloid characteristics on the fabrication of ZnO nanowire arrays by electrophoretic deposition

Y. C. Wang, I. C. Leu* and M. H. Hon

Department of Materials Science and Engineering, National Cheng Kung University, Tainan, Taiwan. E-mail: icleu@mail.ncku.edu.tw

Received 7th December 2001, Accepted 12th April 2002
First published as an Advance Article on the web 15th May 2002

In this study ZnO colloidal suspensions with varied characteristics were synthesized by varying the amount of added sodium hydroxide. The template-mediated preparation for nanosized ZnO arrays was conducted by electrophoretic deposition in the nanochannels of anodic alumina membranes. The effect of colloid characteristics on the deposition of ZnO nanowire arrays was investigated, and the related deposition mechanisms, morphologies and optical properties of the deposits were discussed. The deposited ZnO nanoarrays were characterized by scanning electron microscopy (SEM), transmission electron microscopy (TEM) and photoluminescence (PL) studies. It was found that both the morphology and the deposition rate of ZnO nanowire arrays were influenced by the pH of the suspension and the applied voltage. The particle surface charge and size changed with the pH of the suspension, which in turn affected the deposition characteristics. The deposition rate of nanowire arrays was high at the initial stage and then approached a saturation value. The deposition rate also increased with increasing zeta potential of the particles and the applied voltage for EPD of ZnO nanowires. The photoluminescence properties of ZnO arrays were largely determined by particle size and surface properties of the nanoparticles comprising the nanowire arrays.

Introduction

With the development of various nanometer-sized electronic and photonic devices, high density and well-aligned nanowire arrays exhibit a great potential for fundamental research and practical applications. ZnO as a low-voltage and short wavelength optoelectronic material is the subject of extensive interest. Many methods, which employ the route of template-mediated synthesis, have been proposed to fabricate nanosized fibrils, wires and tubules of materials, such as sol–gel deposition,[1–3] electrochemical deposition[4] and chemical vapor deposition (CVD).[5] There are some advantages and limitations for each of the above methods. However, the electrophoretic deposition (EPD) process proposed here is another effective and controllable method for the fabrication of ZnO nanowire arrays *via* the assistance of an anodic alumina membrane (AAM) template. The advantages of the EPD fabrication process are ease and speed of operation, applicability to many materials,[6] low-cost and highly reproducible characteristics.

EPD has gained world-wide applications for the preparation of coating[7] and laminated materials,[8] and as an infiltration process for composites.[9] EPD is performed, under the influence of an electric field, by the motion of charged particles in a suspension and then deposition on the oppositely charged electrode. It is generally accepted that particulate surface charge is required for stabilizing the suspension during the EPD process. Several authors have studied the stability and zeta potential of powders obtained in organic media.[10] In addition, it was reported that the degree of charge development and its sign are influenced by the pH of the suspension,[11,12] and a stable suspension can be obtained if the surface charge of the particulate is high enough.[12] By studying the pH effect on Al_2O_3 in ethanol, the EPD deposition rate was found to be dependent on pH.[13] The more stable the pH of suspension is, the higher the deposition rate that can be attained. On the other hand, the electric field provides the driving force for the particles to absorb on the electrode. Hence, the pH of the suspension and the voltage exerted on the electrophoretic cell are both important variables in EPD. However, relatively little attention has been paid to the variation of deposition characteristics of nanowires within nanochannels of AAM under the influence of particle surface state and the applied electric field. In this study, we report a process combining the synthesis of ZnO nanoparticles and their colloidal solution preparation and the EPD of ZnO nanowire arrays in AAM by changing both the pH of the suspensions and the applied voltage in order to investigate their deposition characteristics.

Experimental

The synthesis of ZnO colloidal suspensions for EPD followed the method of Bahnemann *et al.*.[14] The ZnO colloidal suspensions were prepared from zinc acetate (ACS reagent grade) in 2-propanol (ACS reagent grade) with NaOH (ACS reagent grade) added to adjust the pH. First, a solution of 5.5×10^{-4} mol of $Zn(OAc)_2 \cdot 2H_2O$ in 80 ml of 2-propanol was prepared at 50 °C. The solution was diluted to 230 ml with 2-propanol and cooled to 0 °C. Then 20 ml of the solution was added with another mixture containing the desired amount of NaOH (the concentration of which was varied from 2.5×10^{-3} to 1.25×10^{-2} M) in 100 ml 2-propanol. In this study the ZnO colloidal suspensions for EPD were obtained with two different concentrations of 2.5×10^{-3} M (solution A) and 1.25×10^{-2} M (solution B) NaOH in 2-propanol. After aging in a water bath at 65 °C for 2 h a transparent suspension of ZnO particles was obtained. Subsequently, the suspensions for EPD were treated by drying at −35 °C for 1 h to increase the particle concentration in the bath. On the other hand, the colloid solution C, which was obtained after 14 days of further aging of solution A at 5 °C, was prepared to investigate the aging and surface charge effect on the growth characteristics of ZnO nanowire arrays. Then 8×10^{-4} M of $Zn(NO_3)_2 \cdot 6H_20$ was added to the suspensions as a binder agent for the EPD process. The AAM templates used for the synthesis of aligned nanowire arrays are commercially available (Whatman, Anodisc). This type of membrane was characterized with 200 nm pore diameter and 10^9–10^{10} (pores cm^{-2}) pore density.

For EPD, a platinum sheet was used as the anode, and an AAM attached to a Cu foil was used as the cathode. A layer of Au was deposited on one side of the AAM and then the coated side of the AAM was attached to Cu foil to enhance the conductivity. ZnO nanowire arrays were deposited at voltages from 10 to 400 V using a regulated dc power supply. The AAM was removed from the colloidal suspension after 5–25 min of deposition and allowed to dry at ambient conditions. For SEM observation and growth rate measurements, the AAM was removed from the ZnO/AAM samples by dissolving the AAM in 0.5 M NaOH solution and washing several times with double-distilled water.

Zeta potentials of the colloids were measured using a Zetasizer 300 HS (Malvern, UK). Optical absorption measurements for the evaluation of quantum confinement effects of the colloids were performed using a UV-VIS spectrometer (Perkin Elmer Lambda 40). Photoluminescence (PL) spectra were measured at room temperature on a spectrometer (HITACHI F-4500) with a Xe lamp as the excitation light source. The morphology of ZnO nanowire arrays was observed using SEM (Phillips XL-FEG SEM) and TEM (JEOL AEM-3010). For TEM analysis, the specimens were prepared by dissolving the assembly with 0.5 M NaOH solution, then dispersing the released ZnO nanowires in alcohol by ultrasonic agitation, and adding dropwise on to carbon-coated copper grids.

Results and discussion

The size and surface state of the particles in the suspension are two important factors in determining the processing of EPD. The dependence of colloid characteristics on the pH of the solution was first investigated. The average particle size was determined from the absorption spectra using the effective mass model derived by Brus.[15,16] In the strong-confinement regime, the confinement energy of the first excited electronic state can be approximated by eqn. (1).

$$E^* \cong E_g^{bulk} + \frac{\hbar^2\pi^2}{2r^2}\left(\frac{1}{m_e^* m_0} + \frac{1}{m_h^* m_0}\right) - \frac{1.8e^2}{4\pi\varepsilon\varepsilon_0 r} - \frac{0.124e^4}{\hbar^2(4\pi\varepsilon\varepsilon_0)^2}\left(\frac{1}{m_e^* m_0} + \frac{1}{m_h^* m_0}\right)^{-1} \quad (1)$$

Here E_g^{bulk} is the bulk band gap, $\hbar$ is Planck's constant, r is the particle radius, m_e* is the effective mass of the electron, m_h* is the effective mass of a hole, m_o is the free electron mass, e is the charge on an electron, ε_o is the permittivity of free space, and ε is the relative permittivity. The particle size was obtained from the band gap inferred from the optical absorption spectra taking $E_g^{bulk} = 3.4$ eV, $m_e^* = 0.24$, $m_h^* = 0.45$, and $\varepsilon = 3.7$.[16]

Using the above equation, Fig. 1 shows the variation of the calculated average particle size for ZnO colloids as a function of the pH of the solution by varying the amount of NaOH added. It shows that the particle size increases with the pH value, with average particle diameters of about 3.6, 4.8 and 4.0 nm for solution A (pH 6.0), B (pH 9.7) and C (pH 6.1), respectively. The results are in agreement with the absorption spectra examined by Sakohara *et al.*,[17] who claimed that the particle size increased with the lithium hydroxide concentration. The average particle size of 4.8 nm for solution B is comparable to the reported value of 5.0 nm measured by TEM observation[14] for particles synthesized using the same process. The slight diameter difference may be due to the inhibition of particle growth at such a low drying temperature (−35 °C for 1 h). According to a previous report,[14] the ZnO particles, prepared by this method, are almost spherical with a relatively narrow particle size distribution ($\Delta R = 0.5$ nm). This indicates that the calculated mean diameter distribution for particles here from eqn. (1) is reasonable. As is evident from Fig. 1, as colloid suspension A is aged for a long time, the average particle size changes from 3.6 to 4.0 nm (designated solution C). It is known from previous study that the aging treatment of ZnO colloids would produce large particles by grain growth.[18] It is concluded that the particle size of the ZnO colloids is dependent on the amount of NaOH added and the aging treatment.

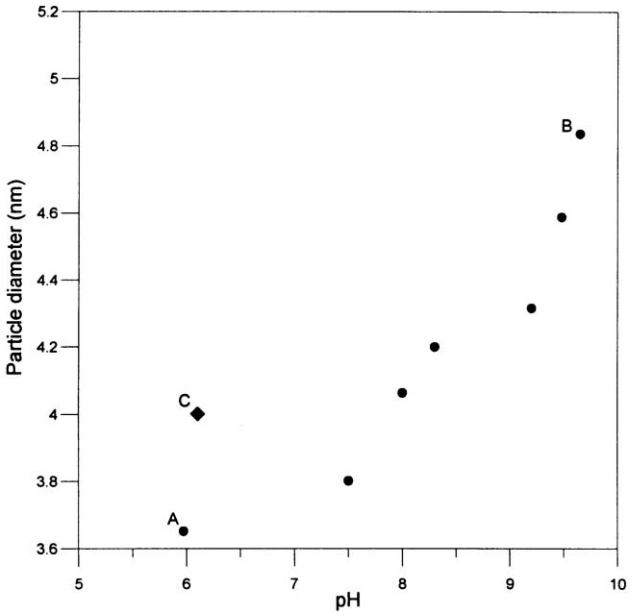

Fig. 1 Relationship between the calculated average particle size and the pH of the ZnO colloidal suspension; symbol (◆) relates to an aged colloid (solution C).

The variation of zeta potential with pH of the ZnO suspensions, plotted in Fig. 2, shows that the zeta potential increases with the pH value. The zeta potentials for solutions A, B and C are +9.0, +24.9 and +11.5 mV, respectively. The ZnO colloidal particles prepared by this method were reported to contain acetate (CH_3COO^-) groups, originating from the reagent, zinc acetate, on their surface.[17] These groups consist of unidentate, bidentate (chelate), and bridging type structures. Upon addition of base, the concentration of acetate groups increases and then the concentration of counter ions[12] around the particles should also increase. Because of the increased amounts of protons and polar molecules[19] that react with the

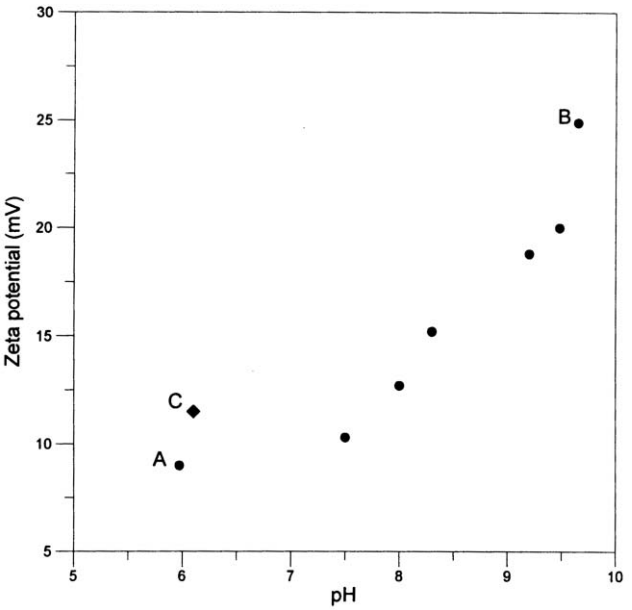

Fig. 2 Dependence of zeta potential on the pH of the ZnO colloidal suspension; symbol (◆) relates to an aged colloid (solution C).

Table 1 Characteristics of ZnO particles under different colloidal conditions

	Ph	Particle size/nm	Zeta potential/mV
Solution A	6.0	3.7	9.0
Solution B	9.7	4.8	24.9
Solution C	6.1	4.0	11.5

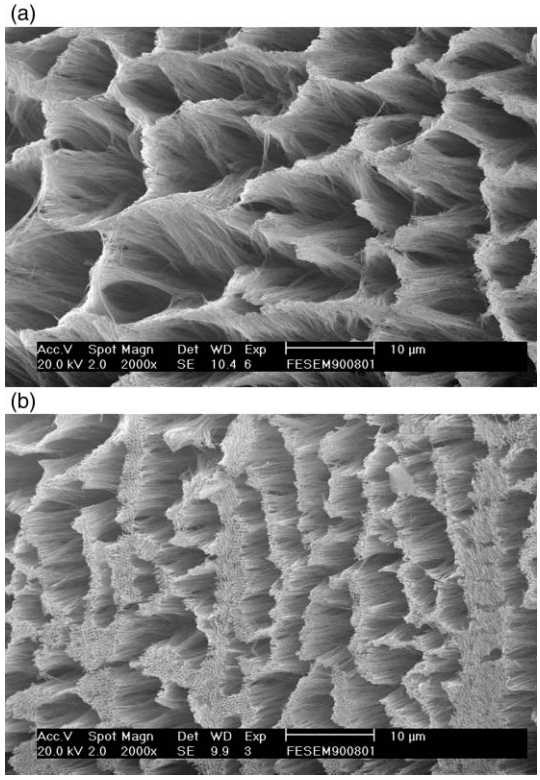

Fig. 3 SEM micrographs of the deposited ZnO nanowire arrays obtained at (a) 20 and (b) 200 V.

double layers of ZnO particles in the suspension, the zeta potential would increase with pH. Therefore, addition of base not only changes the particle size, but also affects the chemistry of the particle surface in the suspension. The relationship between colloidal processing conditions and consequent particle characteristics is summarized in Table 1.

SEM micrographs of the deposited nanosized ZnO arrays obtained at 20 and 200 V are shown in Fig. 3(a) and (b), respectively. It is interesting that the deposited products obtained under different processing parameters have the form of fibrils or tubules with the same length within an array, which demonstrates the processing capability of the EPD in preparing highly aligned and uniform nanosized arrays. For the sol–gel process, a more concentrated precursor should be employed for subsequent gelling in order to fabricate the desired arrays. However, the nanowire arrays obtained from a solution with a low colloid concentration in this study indicates that the EPD process is an efficient process for extracting solid product even from a highly diluted solution.

The percentage of fibrils in ZnO nanowire arrays embedded in AAM as a function of the applied voltage from different suspensions of ZnO colloids is shown in Fig. 4. Three different morphologies due to the voltage-dependent filling characteristics for both high and low zeta potential solutions can be observed, *i.e.*, fibrils, tubules and a mixed product of both. For solution B (high zeta potential), when the voltage was relatively low (10–30 V), only ZnO nanofibrils could be obtained. However, when the deposition voltage was increased to above 60 V, the product changes from fibril to tubule form, and a transition

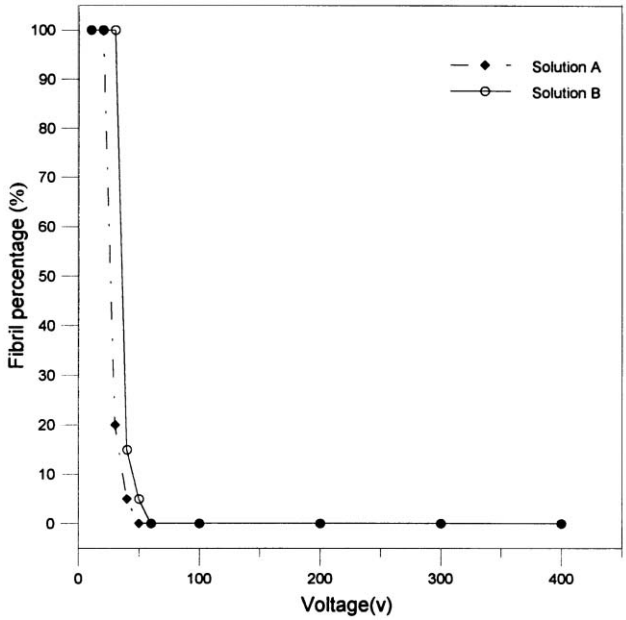

Fig. 4 The percentage of fibrils in ZnO nanowire arrays embedded in AAM as a function of the applied voltage for colloids prepared under different conditions.

region with mixed forms of product occur at intermediate voltages. However, for solution A (low zeta potential), ZnO nanofibrils could only be obtained from 10 to 20 V, and the product changed from fibril to tubule form for voltages above 50 V.

In the EPD process, the success of deposition relies on the following two steps: (i) the movement of charged particles in a suspension to the electrode, and (ii) the formation of a coherent deposit on the electrode surface dependent upon the electrostatic repulsion from the two approaching charged nanoparticles,[20] the London–van der Waals (LVDW) attraction and the driving force applied by the electrical field during EPD.[19] In the present study the ZnO nanoparticles are positively charged, as evidenced from zeta potential measurements. However, the pore walls of the AAM were also reported to be positively charged.[21] At low voltages, because of the electrostatic repulsion between the ZnO particles and the wall of AAM, nanofibrils are first deposited from the base of the channels near the cathode electrode and then extended toward the bulk solution with increasing deposition time.

By contrast, at higher voltages, the high electric field causes dielectric breakdown of the insulating AAM within the solution, which makes the AAM walls carry the same charge as the cathode, and the positively charged particles should absorb preferentially on the pore walls. Therefore, one-side opened tubules were obtained in the AAM. In addition, in the voltage region with mixed product, the curve representing the percentage of fibrils was found to change rapidly with a small variation of voltage. It is believed that such a phenomenon is closely related to the instant conductivity change from negative to positive, which could further support the mechanism mentioned above in controlling the filling characteristics of particles within channels.

The effect of colloidal characteristics on the filling behavior deserves further discussion. At higher zeta potential, the double layer thickness increases, and the particles are more stable against coagulation.[12] It has been reported that, with increased applied voltage to a colloidal suspension, the applied field exerts a force which distorts the double-layer envelope, resulting in a thinner head and an elongated tail to the particles.[12] Therefore, nanoparticles with low zeta potential, which indicates a thin leading double layer, can approach close enough to overcome the electrostatic repulsion between the

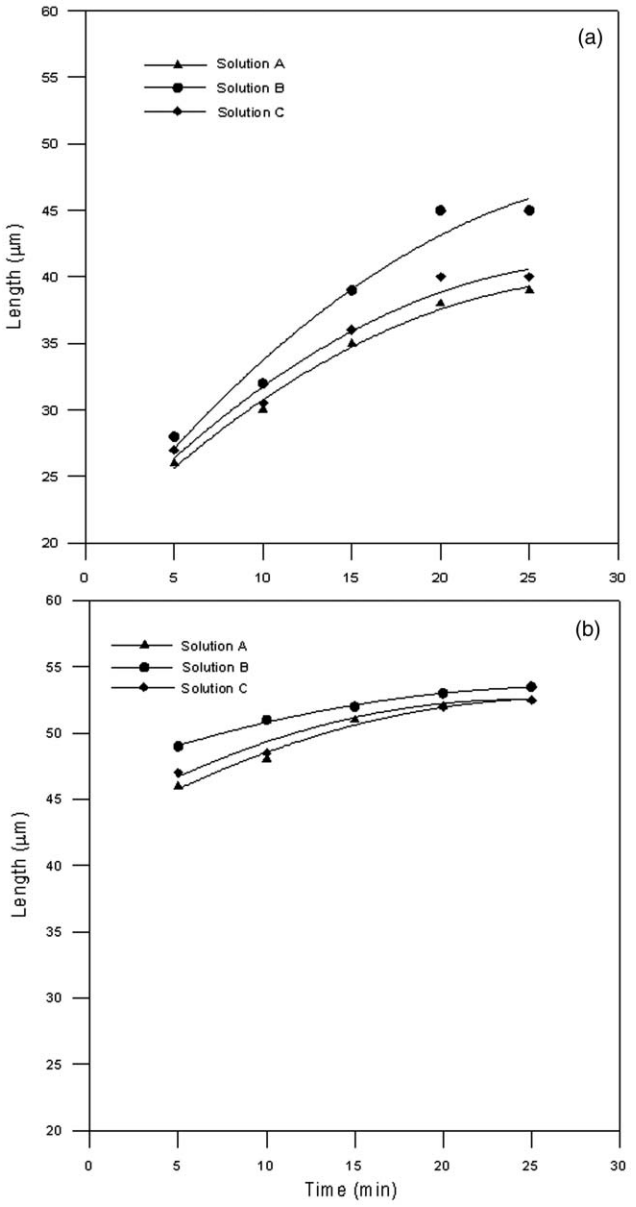

Fig. 5 Relationship between length and deposition time for ZnO nanowire arrays embedded in AAM from solutions A, B and C at (a) 20 V and (b) 200 V.

channel walls of the AAM and the nanoparticles. Hence, the mixed product from the low zeta potential solution (solution A) will be formed earlier than found for the higher zeta potential solution (solution B). This means that the electric field not only influences the double layers close to the powders but also affects the product morphology.

Fig. 5(a) and (b) show the relationship between the length and the deposition time for ZnO nanowire arrays embedded in AAM for solutions A, B and C at applied voltages of 20 and 200 V, respectively. The length increases rapidly at the initial stage and then approaches a saturation value after about 20 min of deposition for all solutions under both high and low applied voltages. It is seen that the length of arrays, after 5 min of deposition, increases with increasing zeta potential (in the order B > C > A) of the colloids and the applied voltage. Particle velocity is the main factor in determining the deposition rate of arrays. As expressed by the Stokes' equation,[22] the particle velocity, v, for a colloid can be estimated according to eqn. (2).

$$v = \frac{ZeE}{6\pi\eta r} \quad (2)$$

Here Z is the charge on the particle, e is the charge on an electron, E is the electric field, η is the viscosity of the solution, and r is the particle radius. For each of the applied voltages, it is considered that the electric field strength is constant for the bulk solution. According to eqn. (2) the velocity of particles increases with the particle charge but decreases with the particle size. Therefore, using the values listed in Table 1, it is predicted that the velocity for the particles moving in solution A is lower by a factor of about 2 than that for solution B. On the other hand, the deposition rates obtained from the slope of the linear region in Fig. 5(a), *i.e.* the region before approaching deposition rate saturation, for solutions B and A are 1.14 and 0.82 μm min^{-1}, respectively. The difference between the particle velocity and array deposition rate can be further accounted for by considering the assumptions in the Stokes' equation or the values used for the constants in eqn. (2).[22] One factor might influence the transport of colloids not considered in the above arguments is the solution viscosity. For example, in our previous study,[23] for more concentrated colloidal suspensions, the higher resulting viscosity will inhibit particle transport in the solution.

From particle size and zeta potential measurements, the net charge carried by the aged particles (solution C) is greater than that of the original suspension (solution A). When 20 V is applied, the fibril deposition rate of the aged solution was slightly higher than that of the original solution. This result indicates that the particle movement towards the cathode was slightly enhanced with increasing zeta potential, therefore facilitating deposition on the cathode. In a study concerning the sedimentation of SiO_2 by EPD, Holgada *et al.*[24] also observed a similar result that the sedimentation rate is increased with increasing zeta potential.

By increasing the applied voltage to 200 V, the length of arrays also increases in the initial stage and then saturates, both at high or low zeta potential conditions (Fig. 5(b)). It is interesting to find that, at high voltage, the initial (< 5 min) deposition rate is higher than that at low voltage, which is believed to be due to the higher driving force and the tubule form of arrays produced at high voltage. However, the deposition rate of nanowires at low voltage is far higher than that at high voltage within the time interval of 5 to 25 min. The variation of the deposition rate for the respective ZnO deposits as a function of deposition time is attributed to the rapidly increased resistance due to the deposited ZnO layer and the depletion of the suspension, which in turn cause the current to decrease correspondingly.[25-27] The increased resistance also reduced the effective electric field acting as the driving force for further deposition, therefore, leading to the appearance of growth saturation with deposition time. As mentioned earlier, the phenomenon of rate saturation was found for both low and high voltage conditions; however, it is far more significant for the latter. As a brief summary, by varying the pH of the colloidal suspension and the aging time, the surface charge and particle size change. However, the results show that the surface charge is more significantly affected and could be the major factor in determining the particle movement as well as the consequent array deposition rate. Comparing the results of Figs. 4 and 5, it is obvious that the surface charge influence is larger than that of the particle size, which can be understood in terms of deposition rate (Fig. 5(a)) and deposit morphology (Fig. 4). In addition, the difference in the deposition rate between different solutions at the applied voltage of 200 V is not significant. Hence, the electric field effect dominates the deposition rate of ZnO nanowire arrays at higher applied voltages.

Fig. 6(a) and (b) show TEM images of a ZnO nanofibril and nanotubule, respectively. It can be seen in Fig. 6(a) that the nanofibrils are located in the center of the cylindrical alumina pores with a diameter of about 50 nm, which is as expected for a proposed deposition mechanism for the preparation of

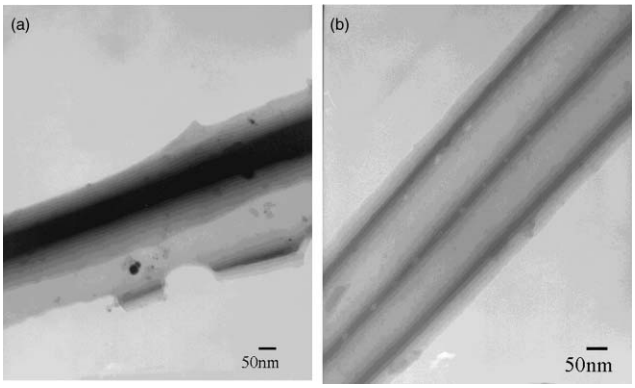

Fig. 6 Typical TEM images for ZnO arrays showing (a) a nanofibril and (b) a nanotubule.

nanowire arrays.[28] In this study nanofibrils of TiO_2 arrays synthesized by the sol–gel method were deposited from the center of the AAM channels due to force balances between particles and channel walls. The present study reveals that for EPD under low voltage, the applied electric field only acts as a driving force to transfer the particles into nanopores of AAM, while the force balance between particles and channel walls remains unchanged. Fig. 6(b) shows a hollow nanotubule with a thin wall and a diameter with about the same dimension as the pore size. The nanotubule has a smooth morphology and longitudinal uniformity in both diameter and wall thickness along the axis. When using high voltage, some voids near the channel walls were observed, which may be due to hydrogen gas evolution at the cathode, or as a result of slight shrinkage due to quick drying after EPD. To overcome such problems, the deposition can be carried out on a hydrogen-absorbing palladium electrode[29] and the deposits can be slowly dried under atmosphere-controlled conditions, respectively. Compared with the nanofibrils prepared by the sol–gel method,[28] the surface smoothness and the uniformity of dimensions have been improved in the present study.

The PL spectra in Fig. 7 for samples from different solutions at an excitation wavelength of 370 nm show that all samples possess two emission peaks at about 380 and 510 nm, but with varied relative intensity and exact location. It was reported that the UV luminescence peak at $\sim$380 nm corresponds to the near

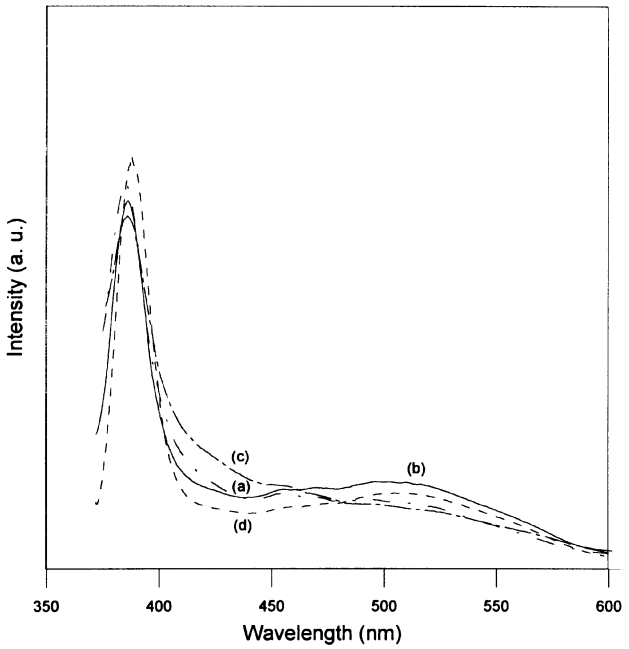

Fig. 7 PL spectra of the ZnO nanowire arrays obtained from various solutions: (a) A, (b) B, (c) A in the absence of $Zn(NO_3)_2{\cdot}6H_2O$ binder and (d) B heated at 400 °C in air for 5 h.

band-edge emission, and the green emission peak at $\sim$510 nm is due to a deep level or trap-state emission.[14,30] The nanowires synthesized by the present technique predominantly exhibit band gap luminescence with a relatively weak green emission, especially from solution A. It was reported that the band gap emission from PL measurement can be an index of good crystal quality[31] and the above result indicates good quality for all the samples obtained. In addition, the band-edge emission blue shifts with decreasing base concentration (381 nm for solution A (Fig. 7(a)) and 385 nm for solution B (Fig. 7(b))), which may be due to reduction in particle size. Fig. 7 also shows that the visible emission of the PL observed in the case of solution A shifts somewhat to shorter wavelengths (about 460 nm) compared with that of 510 nm for solution B. The blue shift in the visible emission with decreasing particle size closely follows the blue shift in the band edge emission, indicating that the two are related.[32]

It is reported that the colloid contains reaction byproducts, such as acetate acid derivatives, absorbed during the preparation process.[17,33] According to IR spectral results by Sakohara *et al.*,[33] the surface complexes that are absorbed to or bonded to the surface of the ZnO nanoparticles may change during heating above 200 °C. The bonding structure of acetate with zinc oxide changes from unidentate to bidentate with increasing firing time. The unidentate complex is believed to trap the photogenerated holes during radiation and thus intensifies the visible luminescence;[34,35] while after heat treatment the concentration of unidentate acetate decreased, which in turn results in a lowered intensity of the visible luminescence. A more detailed investigation regarding the effects of the reaction byproducts on the luminescence spectra intensity needs to be carried out.

Upon comparing the results between Fig. 7(a) and (b), it is evident that the visible luminescence intensity increases with the amount of the hydroxide added to prepare the colloids. The dependence of luminescence intensity on the amount of hydroxide may be a consequence of the amount of unidentate and bridging complexes present on the particle surface, which increases with increasing hydroxide addition and leads to intensified green emission. In agreement with our observation, it is reported that ZnO colloids prepared with a high ratio of zinc acetate/hydroxide contain a higher amount of unidentate and bridging complexes absorbing on the surface of ZnO particles, which was confirmed by IR spectroscopy when the sample was prepared by adding lithium hydroxide as a base for the preparation of zinc oxide.[17]

The visible luminescence properties of the green emission are almost the same whether the sample is in the presence or absence of $Zn(NO_3)_2{\cdot}6H_2O$ added as a binder agent for EPD (*cf.* Fig. 7(a) and (c)). A possible explanation may be the relatively low concentration of Zn^{2+} in the suspension. In addition to the above-mentioned complexes, the presence of impurities may also have an influence on the luminescence properties. However from the X-ray photoelectron spectroscopic results (not shown here), except for carbon, no other impurity is observed in the XPS spectrum. The presence of carbon is due to adventitious carbon contamination from air and acetate derivatives. The results clarify the dependence of luminescence on the concentration of Zn^{2+} ion and the presence of complex, and it is concluded that the emission peaks are predominantly influenced by the acetate complex when only relatively small amount of the Zn^{2+} ions absorb on ZnO particles, as shown in Fig. 7(a)–(c).

Moreover, the effect of heat treatment on the PL of the sample has also been studied and it was found that a heat treatment step caused a decrease in the intensity of the green emission, and the band gap emission peaks slightly red shifted as compared with that of the as-prepared sample, as shown in Fig. 7(d). This may be attributed to the decrease of the amount of singly ionized oxygen vacancies in ZnO[36] and grain growth[18] with a heat treatment step. In addition, the presence of stronger

near band edge luminescence of the sample after heat treatment was observed, which may demonstrate the better quality of the ZnO nanoparticle sample *via* surface improvement (*i.e.* the number of singly ionized oxygen vacancies is reduced by oxygen compensation from air).[31] Bidentate surface coordination was reported to lead to trapping of electrons and quenching the visible luminescence.[34,35] It is believed that due to the presence of the absorbed bidentate acetate, and reaction with oxygen from air, the luminescence intensity is decreased after heat treatment in the present study.

Conclusions

Uniform and aligned ZnO nanowire arrays embedded in AAM were fabricated by combining the colloid preparation and EPD process. The morphology of ZnO nanowire arrays and the deposition rate are influenced by the pH of the suspension and the applied voltage. The pH of suspension not only changes the particle size, but also affects the chemistry of the particle surface. On the other hand, the applied voltage acts to provide the driving force for particles to deposit on the cathode, as well as thinning the double layer, and thus changes the deposition morphology. The deposition rate is high at the initial stage of deposition but later saturates. The deposition rate increases with applied voltage and zeta potential of the particles. Besides, under a given electric field, the zeta-potential effect is higher than that of the particle size in determining the deposition rate of ZnO nanowire arrays under the parameters employed in the present study. The band gap luminescence is predominant for ZnO arrays synthesized by the EPD process, while the intensity of the green emission luminescence decreases after heat treatment. The photoluminescence is progressively blue shifted with decreasing particle size, and the surface properties of ZnO particles are found to influence the green emission.

Acknowledgement

The authors gratefully acknowledge the financial support by the National Science Council of Taiwan, ROC (Grant No. NSC 90-2216-E-006-039)

References

1 Y. Hamasaki, S. Ohkubo, K. Murakami, H. Sei and G. Nogami, *J. Electrochem. Soc.*, 1994, **141**, 660.
2 B. B. Lakshmi, P. K. Dorhout and C. R. Martin, *Chem. Mater.*, 1997, **9**, 857.
3 Y. Lei, L. D. Zhang, G. W. Meng, G. H. Li, X. Y. Zhang, C. H. Liang, W. Chen and S. X. Wang, *Appl. Phys. Lett.*, 2001, **78**, 1125.
4 Y. Li, G. W. Meng and L. D. Zhang, *Appl. Phys. Lett.*, 2000, **76**, 2011.
5 J. C. Hulteen and C. R. Martin, *J. Mater. Chem.*, 1997, **7**, 1075.
6 O. O. Van der Biest and L. J. Vandeperre, *Annu. Rev. Mater. Sci.*, 1999, **29**, 327.
7 P. E. Pierce, *J. Coat. Technol.*, 1981, **53**, 52.
8 P. S. Nicholson, P. Sarkar and X. Huang, *J. Mater. Sci.*, 1993, **28**, 6274.
9 L. Gal-Or, S. Haber and S. Liubovich, *J. Electrochem. Soc.*, 1992, **139**, 1078.
10 H. Kennedy and A. Foissy, *J. Electrochem. Soc.*, 1977, **60**, 33.
11 P. Sarkar and P. S. Nicholson, *J. Am. Ceram. Soc.*, 1996, **79**, 1987.
12 J. S. Reed, in *Introduction to the Principles of Ceramic Processing*, John Wiley & Sons, New York, 1986, p. 142.
13 B. EI-Jazairi, D. White and J. P. Roberts, in *Science of Ceramics*, vol. 9, Nederlandse Keramisch Vereniging, 1977, p. 46.
14 D. W. Bahnemann, C. Kormann and M. R. Hoffmann, *J. Phys. Chem.*, 1987, **91**, 3789.
15 L. E. Brus, *J. Chem. Phys.*, 1983, **79**, 5566.
16 L. E. Brus, *Nanostruct. Mater.*, 1992, **1**, 71.
17 S. Sakohara, M. Ishida and M. A. Anderson, *J. Phys. Chem. B*, 1998, **102**, 10169.
18 L. Spanhel and M. A. Anderson, *J. Am. Chem. Soc.*, 1991, **113**, 2826.
19 P. S. Nicholson and P. Sarkar, in *Ceramic Processing Science and Technology*, ed. H. Hausner, G. L. Messing and S.-I. Hirano, American Ceramic Society, Westerville, OH, 1995, p. 469.
20 M. Trau, D. A. Saville and I. A. Aksay, *Science*, 1996, **272**, 706.
21 J. W. Diggle, T. C. Downie and C. W. Goulding, *Chem. Rev.*, 1969, **69**, 365.
22 P. C. Hiemenz and R. Rajagopalan, in *Principles of Colloid and Surface Chemistry*, Marcel Dekker, New York, 3rd edn., 1997, p. 62.
23 Y. C. Wang, I. C. Leu and M. H. Hon, *J. Cryst. Growth*, in press.
24 M. Holgada, F. Garcia-Santamaria, A. Blanco, M. Ibisate, A. Cintas, H. Miguez, C. J. Serna, C. Molpeceres, J. Requena, A. Mifsud, F. Meseguer and C. Lopez, *Langmuir*, 1999, **15**, 4701.
25 C. Kawai and S. Wakamatsu, *J. Mater. Sci.*, 1996, **31**, 2165.
26 P. Sarkar and P. S. Nicholson, *J. Am. Ceram. Soc.*, 1996, **79**, 1897.
27 A. Sussman and T. J. Ward, *RCA Rev.*, 1981, **42**, 178.
28 Y. Lei, L. D. Zhang, G. W. Meng, G. H. Li, X. Y. Zhang, C. H. Liang, W. Chen and S. X. Wang, *Appl. Phys. Lett.*, 2001, **78**, 1125.
29 P. J. Mitchell and G. D. Wilcox, *Nature*, 1992, **357**, 395.
30 M. H. Huang, Y. Wu, H. Feick, N. Tran, E. Weber and P. Yang, *Adv. Mater.*, 2000, **13**, 113.
31 L. Guo, S. Yang, C. Yang, P. Yu, J. Wang, W. Ge and G. K. L. Wong, *Appl. Phys. Lett.*, 2000, **76**, 2901.
32 E. M. Wong and P. C. Searson, *Appl. Phys. Lett.*, 1999, **74**, 2939.
33 S. Sakohara, L. D. Tickanen and M. A. Anderson, *J. Phys. Chem.*, 1992, **96**, 11086.
34 G. J. Meyer, G. C. Lisensky and A. B. Ellis, *J. Am. Chem. Soc.*, 1988, **110**, 4914.
35 M. Anpo, M. Tomonari and M. A. Fox, *J. Phys. Chem.*, 1989, **93**, 7300.
36 K. Vanheusden, W. L. Warren, C. H. Seager, D. R. Tallant, J. A. Voigt and B. E. Gnade, *J. Appl. Phys.*, 1996, **79**, 7983.